

CHEMISTRY

A European Journal

A Journal of



Accepted Article

Title: Uncommon Optical Properties and Silver-responsive Turn-off/on Luminescence in a Pt(II) heteroleptic dithiolene complex

Authors: Salahuddin S. Attar, Flavia Artizzu, Luciano Marchiò, Davide Espa, Luca Pilia, Maria Francesca Casula, Angela Serpe, Maddalena Pizzotti, Alessio Orbelli Biroli, and Paola Deplano

This manuscript has been accepted after peer review and appears as an Accepted Article online prior to editing, proofing, and formal publication of the final Version of Record (VoR). This work is currently citable by using the Digital Object Identifier (DOI) given below. The VoR will be published online in Early View as soon as possible and may be different to this Accepted Article as a result of editing. Readers should obtain the VoR from the journal website shown below when it is published to ensure accuracy of information. The authors are responsible for the content of this Accepted Article.

To be cited as: *Chem. Eur. J.* 10.1002/chem.201801697

Link to VoR: <http://dx.doi.org/10.1002/chem.201801697>

Supported by
ACES

WILEY-VCH

Uncommon Optical Properties and Silver-responsive Turn-off/on Luminescence in a Pt(II) heteroleptic dithiolene complex

Salahuddin S. Attar,^[a] Flavia Artizzu,^[b] Luciano Marchiò,^{*[c]} Davide Espa,^[a] Luca Pilia,^[d] Maria F. Casula,^[a] Angela Serpe,^[e] Maddalena Pizzotti,^[f] Alessio Orbelli Biroli^[g] and Paola Deplano^{*[a]}

Abstract: The complex [Pt(*i*-Pr₂pipdt)(Quinoxdt)] (*i*-Pr₂pipdt = 1,4-diisopropyl-piperazine-2,3-dithione; Quinoxdt= [1,4]dithiino[2,3-*b*]quinoxaline-2,3-dithiolate) exhibits a remarkable green emission at 570 nm (room temperature), which is above the lowest excited state. The complex is characterized by negative solvatochromism as well as a high second-order polarizability. Addition of Ag(I) ions induces i) hypsochromic shift of the lowest frequencies; and ii) reversible quenching of luminescence. The corresponding Ni and Pd complexes have been also prepared and investigated to assist interpretation of optical properties within the triad. Computational studies based on density functional theory and time-dependent theory highlight the electronic properties of [Pt(*i*-Pr₂pipdt)(Quinoxdt)]. The preferential site of interaction between the Pt complex and incoming Ag(I) is evidenced by shape of the Fukui functions, pointing to the thiolic sulfur and platinum atoms as the most reactive sites towards a soft cation. Calculated optical properties are in agreement with experimental findings. This study contributes to shed light on

the structure-properties relationship for this class of compounds

Introduction

Homoleptic and heteroleptic metal dithiolene complexes feature peculiar electronic structures, which result in relevant properties for several applicative fields proper of molecular materials.^[1a-c] Square-planar heteroleptic d⁸ metal-dithiolene complexes have been shown to be suitable candidates to work as tunable second-order nonlinear optical (NLO) chromophores.^[2] The requirement to obtain this property is the presence of two ligands occurring in formally different oxidation states, one reducing (dianionic dithiolate, electron donor), and the other oxidizing (neutral dithione, electron acceptor). These non-centrosymmetric molecules exhibit an absorption peak in the visible spectral region, which is tunable with the HOMO-LUMO energy gap. Specifically, the donor gives a prevailing contribution to the HOMO, and the acceptor mainly contributes to the LUMO, with the coordinated metal acting as a σ -bridge for the electron transfer. Accordingly, the Charge Transfer (CT) donor-acceptor process produces a decrease of the dipole moment from the ground to the excited state and, as a consequence, negative solvatochromism and first hyperpolarizability ($\chi^{(1)}$) is observed.^[3]

Interestingly, the extensively investigated dithione-dithiolate complexes, including [Pt(*i*-Pr₂pipdt)(dmit)] (dmit= 2-thioxo-1,3-dithiole-4,5-dithiolate), do not exhibit luminescence in solution at room temperature or in glassy solvents at 77 K.^[4] On the other hand, heteroleptic platinum diimine-dithiolate (diimine: acceptor, dithiolate: donor) exhibit both 2nd NLO activity and luminescence associated with the CT transition.^[5] Recently, we have reported both homoleptic and heteroleptic platinum complexes with the Quinoxdt ligand (donor) that are emissive in solution and at room temperature (RT). Remarkably, it was observed that the emission falls above the energy of the lowest-energy absorption, $\lambda_{em} > \lambda_{ab}$ (Figure S1).^[6] In the homoleptic case, [Pt(Quinoxdt)₂] (see Figure 1), irradiation at 420 nm yields an emission peak at 572 nm, well above in energy to the lowest absorption peak at 1085 nm, which is $\lambda_{em} > \lambda_{ab}$.^[7] In the heteroleptic case, the [Pt(MBA)(Quinoxdt)] complex (MBA: (R)-MBA-dithioamide),^[8] upon irradiation at 450 nm, shows switchable proton-dependent photoluminescence emission tunable from deep red (715 nm) to bright green (570 nm) as a function of pH. Interestingly, both complexes do not exhibit photoluminescence upon excitation either in the UV region or at the lowest absorption band, which corresponds to the

[a] Dr S. S. Attar, Dr D. Espa, Prof M. F. Casula, Prof P. Deplano
Department of Chemical and Soil Sciences
University of Cagliari, INSTM Research Unit
09042 Monserrato (CA), Italy
E mail: deplano@unica.it

[b] Dr F. Artizzu
L³. Luminescent Lanthanide Lab, Department of Chemistry
Ghent University
Krijgslaan 281 . building S3, B-9000 Gent, Belgium

[c] Prof L. Marchiò
Dipartimento di Scienze Chimiche, della Vita e della Sostenibilità
Ambientale
Università di Parma
Parco Area delle Scienze 11/a, 43124 Parma, Italy
E-mail: luciano.marchio@unipr.it

[d] Dr L. Pilia
Dipartimento di Ingegneria Meccanica, Chimica e dei Materiali
Università di Cagliari
Via Marengo 2, 09123 Cagliari, Italy

[e] Dr A. Serpe
Dipartimento di Ingegneria Civile, Ambientale e Architettura
Università di Cagliari
Via Marengo 2, 09123 Cagliari, Italy

[f] Prof M. Pizzotti
Department of Chemistry, INSTM Research Unit,
University of Milan
Via C. Golgi 19, 20133 Milano, Italy

[g] Dr A. Orbelli Biroli
Istituto di Scienze e Tecnologie Molecolari del CNR (CNR-ISTM),
SmartMatLab Centre,
CNR
Via C. Golgi 19, 20133 Milano, Italy 1

Supporting information for this article is given via a link at the end of the document. **(Please delete this text if not appropriate)**

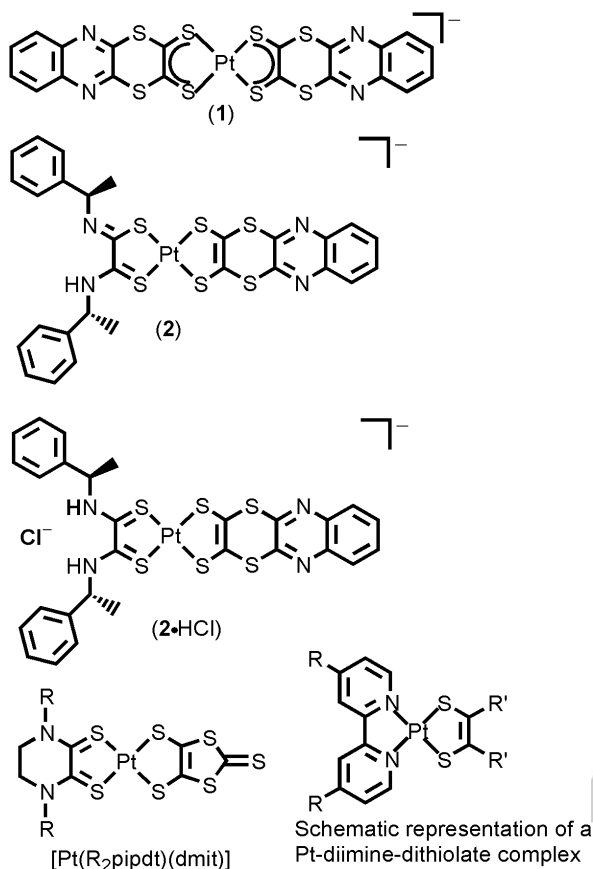


Figure 1: Homoleptic and heteroleptic Pt-dithiolenes. **1**, **2** and **2·HCl** exhibit luminescence in solution at RT, with apparent anti-Kasha behavior.

compound) transitions, respectively. The sequence of the calculated molecular orbitals suggested the intraligand charge-transfer (ILCT) nature of the process, involving orbitals of the dithiolate moiety (Quinoxdt). The RT decay times estimated in the picosecond range and the rather low quantum yields (in the 1×10^{-4} – 10^{-5} range) pointed out that the radiative decay channel is strongly quenched by other deactivation pathways and that the phenomenon related to the observed spectral features can be ascribed to the poor overlap between the superior Quinoxdt-based (LUMO+1) emissive state and the vicinal energy states (related to the LUMO). This orbital mismatch would promote the radiative decay from the high-energy state to the ground state to be competitive with internal conversion.

In this work we elucidate the uncommon optical behaviour of heteroleptic metal dithiolenes by investigating a new heteroleptic platinum-dithiolenes complex, [Pt(*i*-Pr₂pipdt)(Quinoxdt)] (**3a**). In the design, Quinoxdt is purposely maintained, while the acceptor ligand is a neutral dithiooxamide: *i*-Pr₂pipdt (1,4-diisopropyl-piperazine-2,3-dithione). As discussed earlier, the similar [Pt(*i*-Pr₂pipdt)(dmit)] complex is not emissive,

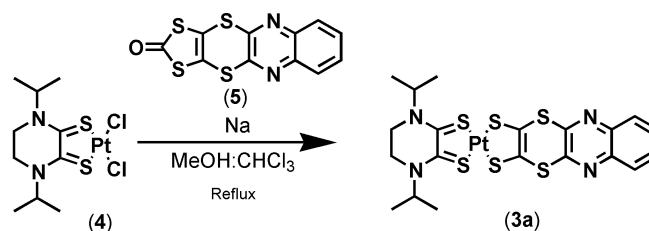
pointing to the prominent role of the Quinoxdt to the optical properties of its complexes.^[3a,4a,b] For clarity reasons the cited complexes are illustrated in Figure 1. Here we report the linear and non-linear optical properties of **3a**, together with a detailed description of the electronic features as derived by density functional theory (DFT), and time-dependent DFT (TD-DFT) calculations. In order to perturb the optical features of **3a**, we have employed Ag(I) in the form of silver triflate, given the presence of a large number of potentially interacting sites on the molecular surface of **3a** with soft cations such as Ag(I). Interestingly, **3a** behaves as a cation luminescent sensor, where emission can be reversibly switched off/on in the presence/absence of Ag(I). The corresponding Ni (**3b**) and Pd (**3c**) complexes have been also prepared and investigated to assist interpretation of uncommon optical properties exhibited by **3a**.

The reactivity indices (Fukui functions)^[9] pointed out the preferred interaction sites in the formation of the **3a**: Ag adduct with 1:2 ratio. Related calculated properties have been found in very good agreement with experimental findings providing new insights into the origin of the unusual optical behaviour of these complexes.

Results and Discussion

[Pt(II)(*i*-Pr₂pipdt)(Quinoxdt)] complex **3a** was prepared as shown in Scheme 1. Accordingly, the precursor [Pt(II)(*i*-Pr₂pipdt)(Cl)₂] (**4**) was added to a solution of disodium [1,4]dithiino[2,3-*b*]quinoxaline-2,3-bis(thiolate) (**5**), prepared *in situ* as detailed in Experimental Section. Green microcrystals of the neutral complex precipitated as the reaction proceeded. Crystals suitable for single crystal X-ray diffraction were obtained by the diffusion method using DMF as solvent and diethyl ether as anti-solvent. Palladium and nickel complexes were prepared by adapting the above procedure, as described in the Experimental Section.

The molecular structure of [Pt(*i*-Pr₂pipdt)(Quinoxdt)]·DMF is reported in Figure 2. The metal geometry is square planar according to the presence of four sulfur atoms from two S,S bidentate ligands. As reported for similar systems formally comprising a dithione (*i*-Pr₂pipdt) and a dithiolate (Quinoxdt) ligands,^[3a-b, 10a-b] the metal-sulfur bond distances are in the very narrow range of 2.277(2)–2.301(2) Å, which is possible to infer the electronic properties of the ligands by purely geometric



Scheme 1. Synthesis of [Pt(*i*-Pr₂pipdt)(Quinoxdt)].

FULL PAPER

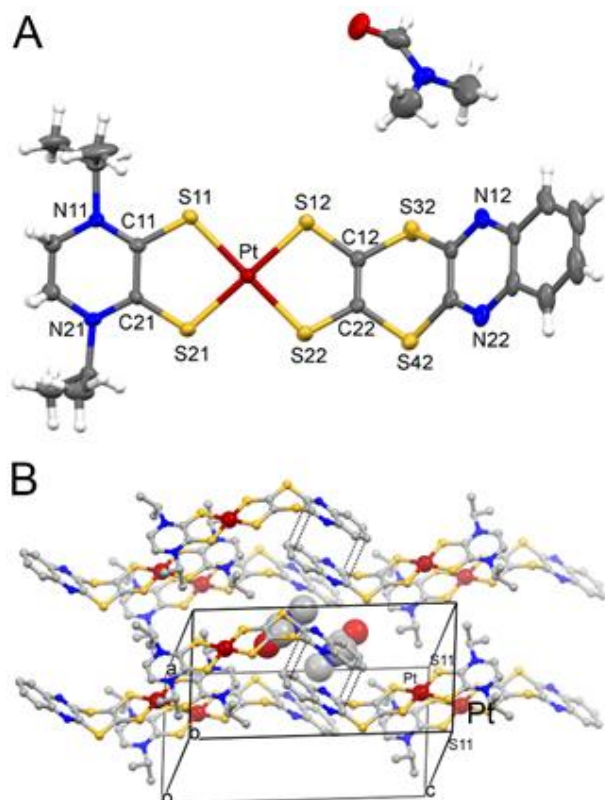


Figure 2: (a) Molecular structure of [Pt(*i*-Pr₂pipdt)(Quinoxdt)]DMF (**3a**·DMF) with thermal ellipsoids drawn at the 30% probability level. (b) Portion of the crystal packing of **3a**·DMF. DMF molecules are depicted in the spacefill style. Selected geometric parameters (Å) for **3a**·DMF: Pt-S(11) = 2.279(2); Pt-S(21) = 2.278(2); Pt-S(12) = 2.279(2); Pt-S(22) = 2.277(2); C(11)-S(11) = 1.691(7); C(21)-S(21) = 1.688(7); C(12)-S(12) = 1.749(7); C(22)-S(22) = 1.743(7); C(11)-C(21) = 1.444(9); C(31)-C(41) = 1.34(1).

parameters such as the M-S bond distances. Nevertheless, the C-S bond distances in *i*-Pr₂pipdt are in agreement with a dithione structure, whereas the C-S bond distances in Quinoxdt are associated to a dithiolate type of structure. Likewise, the C-C bond linked to the coordinated sulfur atoms, exhibits a double bond character for *i*-Pr₂pipdt and a single bond character for the Quinoxdt. The crystal packing of **3a**·DMF is depicted in Figure 2b. The molecules are partially stacked with the peripheral Quinoxdt fragment forming a weakly interacting supramolecular dimer. On the other hand, the fragment comprising the metal center and the *i*-Pr₂pipdt ligand are marginally superimposed, with the two closest contact occurring through the Pt and the S(11) atoms of two symmetry related molecules (3.86 Å). The DMF molecules are located into a pocket delimited by six Quinoxdt moieties and by the methyl groups four *i*-Pr₂pipdt residues. The electronic absorption spectrum of **3a** in DMF solution shows two bands, one is in the vis-NIR region at 836 nm, and the

Table 1. Summary of X-ray crystallographic data for **3a**·DMF.

Empirical formula	C ₂₃ H ₂₉ N ₅ S ₆ PtO
Formula weight	778.96
Temperature/K	240(2)
Crystal system	triclinic
Space group	<i>P</i> -1
<i>a</i> /Å	9.017(1)
<i>b</i> /Å	9.237(1)
<i>c</i> /Å	18.037(2)
α /°	79.282(2)
β /°	86.132(2)
γ /°	72.614(2)
Volume/Å ³	1408.5(3)
<i>Z</i>	2
calc. ρ /cm ³	1.837
μ /mm ⁻¹	5.453
<i>F</i> (000)	768.0
Crystal size/mm ³	0.18 × 0.11 × 0.05
Radiation	Ti K α (1.0407 Å)
<i>G</i> /mm ⁻¹	4.598 to 50.71
Index ranges	-1 ≤ <i>h</i> ≤ 1, -1 ≤ <i>k</i> ≤ 1, -1 ≤ <i>l</i> ≤ 1
Reflections collected	15616
Independent reflections	5144 [<i>R</i> _{int} = 0.0676, <i>R</i> _{sigma} = 0.0746]
Data/restraints/parameters	5144/0/331
Goodness-of-fit on <i>F</i> ²	1.003
<i>R</i> ₁ = $\sum F_o - F_c / \sum F_o$	<i>R</i> ₁ = 0.0422, <i>wR</i> ₂ = 0.0783 [a]
Largest diff. peak/hole / e Å ⁻³	0.61/-0.68

[a] $R_1 = \frac{\sum |F_o - F_c|}{\sum F_o}$, $wR_2 = \frac{[\sum w(F_o - F_c)^2]}{[\sum w(F_o)^2]}^{1/2}$, $w = 1/[\sigma^2(F_o) + (aP)^2 + bP]$, where $P = [\max(F_o, 2)]/3$.

second one occurs at 370 nm. An additional shoulder is found around 500 nm. The peak at lower frequency shows negative solvatochromic behaviour, as reported in Figure 3, in agreement with a decrease of the dipolar moment in the excited state. These findings are in accordance to what is generally observed in metal-d⁸ heteroleptic dithione/ or diimine/dithiolate complexes, which have been largely investigated by us,^[2-3,8-10] by the $\pi \rightarrow \pi^*$ transition^[1a-b] and by others^[12a-b] also for their potential use in photonics.

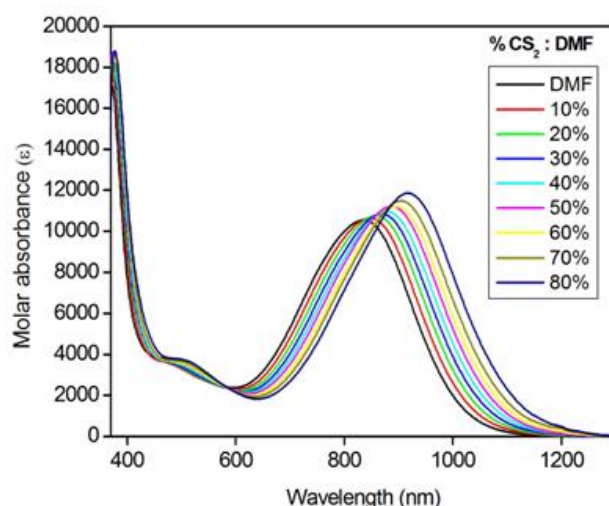


Figure 3: Solvatochromic behaviour of **3a** in DMF/CS₂ mixtures ranging from DMF 100% to 20%.

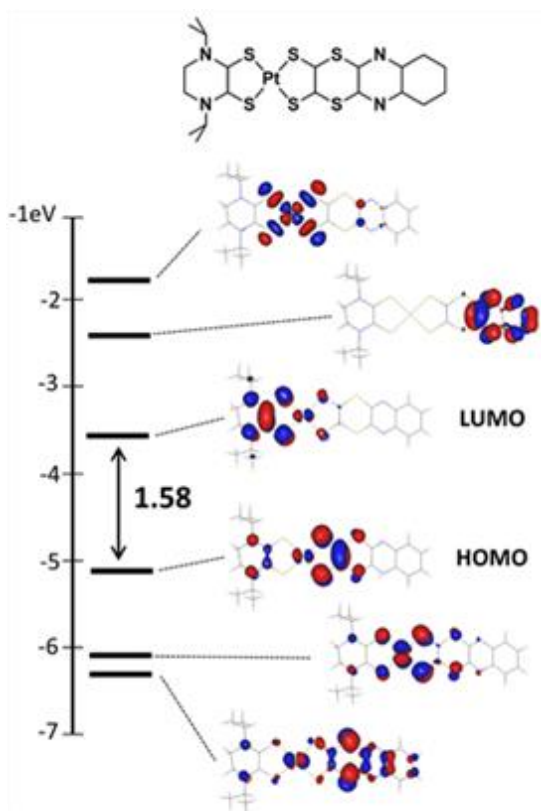


Figure 4: Frontier molecular orbitals of **3a** in the solution phase, DMF, (B3LYP/6-31+G(d)-SDD). For the DFT optimized structure see Figure S2.

The electronic structure of **3a** was investigated by means of DFT methods taking into account the solvent (DMF) by using the polarizable continuum method (PCM). The frontier orbitals are reported in Figure 4. More specifically, the HOMO and LUMO are both formed from the out-of-plane antisymmetric interactions between the metal orbital and a ligand based C2S2 orbital. The HOMO is mainly localized on the dithiolate system, whereas the LUMO is mainly localized on the dithione fragment, in agreement with previous findings for similar systems.^[3] Figure 5 reports the simulated UV-vis spectrum of **3a** together with the twenty first singlet transitions responsible for the main absorption band in the visible region.

The obtained results support that the experimental band at 370 nm is associated to various transitions of low intensity, but it is more detail, and according to the shape of the frontier orbitals, the experimental band at 836 nm can be described as a metal-ligand-to-ligand charge transfer (MLCT) transition centered at 370 nm, Figure 5. The band at approximately 520 nm is associated to various transitions of low intensity, but it is more detail, and according to the shape of the frontier orbitals, the experimental band at 836 nm can be described as a metal-ligand-to-ligand charge transfer (MLCT) transition centered at 370 nm, Figure 5. The band at approximately 520 nm is associated to various transitions of low intensity, but it is more detail, and according to the shape of the frontier orbitals, the experimental band at 836 nm can be described as a metal-ligand-to-ligand charge transfer (MLCT) transition centered at 370 nm, Figure 5.

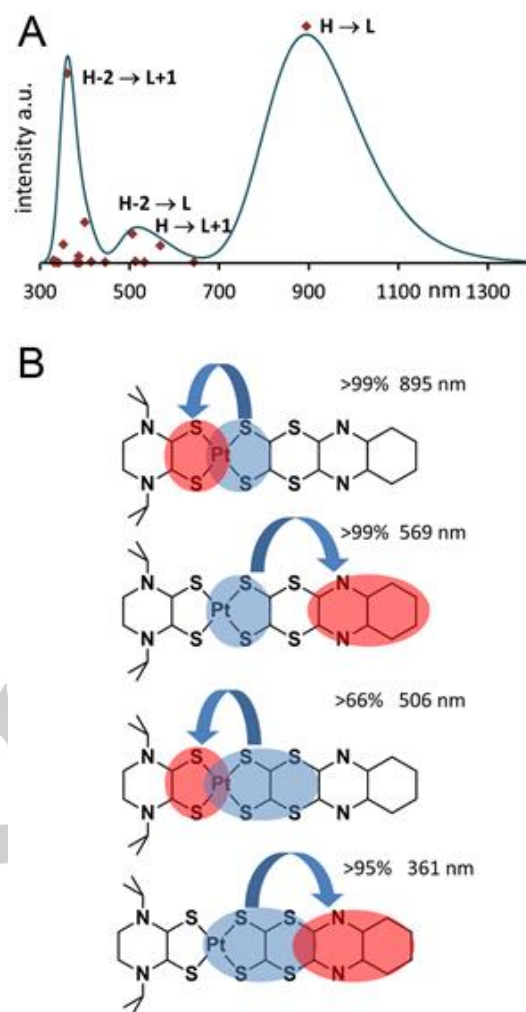


Figure 5: (A) Simulated UV-vis spectrum of **3a** together with the principal singlet transition responsible for the main absorption band in the visible region (red dots). Calculation were performed with the PCM method (DMF), B3LYP/6-31+G(d)-SDD. (B) Depiction of the molecular fragments contributions to the calculated electronic transitions.

components, metal and ligands, see Figure 5. It is worth noting that a similar sequence of MOs is found in [Pt(MBA)(Quinoxdt)] \cdot HCl,^[8] in agreement with similar optical features in the two complexes. Interestingly, [Pt(R₂pipdt)(dmit)]^[3a, 10a-c] exhibits a similar HOMO-LUMO gap, in accordance with the similar wavelengths of the related absorption peaks. This observation is in line with the nature of the three complexes, since they all comprise a donor ligand (Quinoxdt or dmit) and an acceptor ligand (MBA or R₂pipdt) with very similar structure of the HOMO and LUMO orbitals as shown in Figure S3. Treatment of a solution of **3a** in DMF with increasing amount of a silver triflate solution produces a change of the absorption spectra until the 1:2 ratio between **3a** and Ag(I) is achieved, suggesting the formation of a 1:2 adduct, as shown in Figure 6. Unfortunately, any attempt to isolate and characterize the new species failed. Given the features of the absorption spectra, we tentatively suggest that the shift of the lowest energy peak to

FULL PAPER

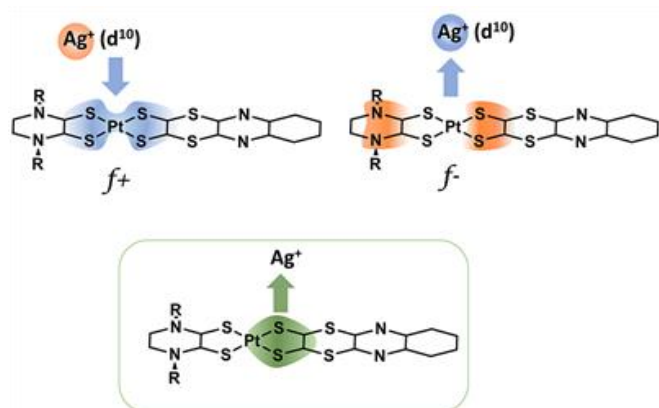


Figure 8: Preferential site of interaction of the molecular surface of **3a** and Ag(I) according to the shape of the positive and negative Fukui function f_+ and f_- .

attack, respectively. According to the f_+ , the atoms involved in the coordination interaction (sulfur atoms and Pt) are suitable to interact with an electron rich environment (nucleophilic attack). On the other hand, the shape of f_- points to the N-C fragment of the dithione together with the C-S of the dithiolato ligand as potential donor groups towards an electrophile (electrophilic attack), Figure 8. Ag(I) can be regarded as a Lewis acid (electrophile) but at the same time it is a soft d^{10} species potentially acting as a nucleophile. Taking these aspects together, the best interacting site for Ag(I) can be identified with the sulfur of the thiolate group. The N atoms of the dithione can also provide a stabilizing interaction with an incoming Ag(I), but there is considerable steric hindrance deriving from the *i*Pr residues. Therefore, as indicated above (see Figure S7), two molecular structures comprising two silver cations and **3a**, were considered for geometry optimization: **3a-trans-Ag₂** and **3a-cis-Ag₂**, which exhibit the two Ag-triflate fragments on the opposite side and on the same side, respectively, of the Pt coordination plane (Figure S7). The optimized adduct **3a-trans-Ag₂**, shown in Figure 9, shows the two silver cations in an almost linear geometry bound by a thiolate sulfur atom and a monodentate triflate anions. The molecular geometry suggests also the presence of a Pt-Ag interaction since the distances between the two metals is shorter than the van der Waals radii sum (~ 3.45 Å),^[20] and it is close to 2.9 Å. In the optimized adduct **3a-cis-Ag₂**, the two silver cations exhibit a different geometry, as the compound is less symmetric than **3a-trans-Ag₂**. In fact, one Ag(I) shows a linear geometry and the second is in a distorted tetrahedral environment. One triflate anion is bridging between the two silver atoms (Figure S7). The computed absorption properties of the two adducts evidence a hypsochromic shift of the low energy band found at 861 nm in **3a** pointing to the role of the Ag-S/Ag-Pt interaction in modulating the absorption feature of the complex, Figure 10 and Figure S9. Nevertheless, **3a-trans-Ag₂** exhibits computed spectral features that are remarkably similar to the experimental findings, and this species can therefore be considered as a good model for the Ag(I)-**3a** adduct in DMF. The hypsochromic shift in **3a-trans-Ag₂** and **3a-**

cis-Ag₂ can be explained by a significant HOMO stabilization because of the thiolate-silver interaction. Moreover, it is worth to note that the nature of the LUMO+1 orbital is changed on interaction with silver ions. In particular, the Quinoxdt-centered MO, which is believed to be associated with the emissive properties of the compound, now occupies the LUMO+2 position in the orbital sequence, in close energy match with the LUMO+1 (Figure S10). Therefore, an additional efficient non-radiative decay channel through d_g^* orbitals is provided, and this is in agreement with the observed luminescence quenching upon addition of silver triflate.

The collective observation of the luminescence properties of **3a-c** seem to further strength our proposal that the emissive state has ILCT (Quinoxdt) character. In fact in the Ni and Pt case similar emission wavelengths by the closely related Quinoxdt complexes (and also from the Quinoxdt ligand precursor) are observed differently to the Pt(II) diimine-dithiolato case. As said,

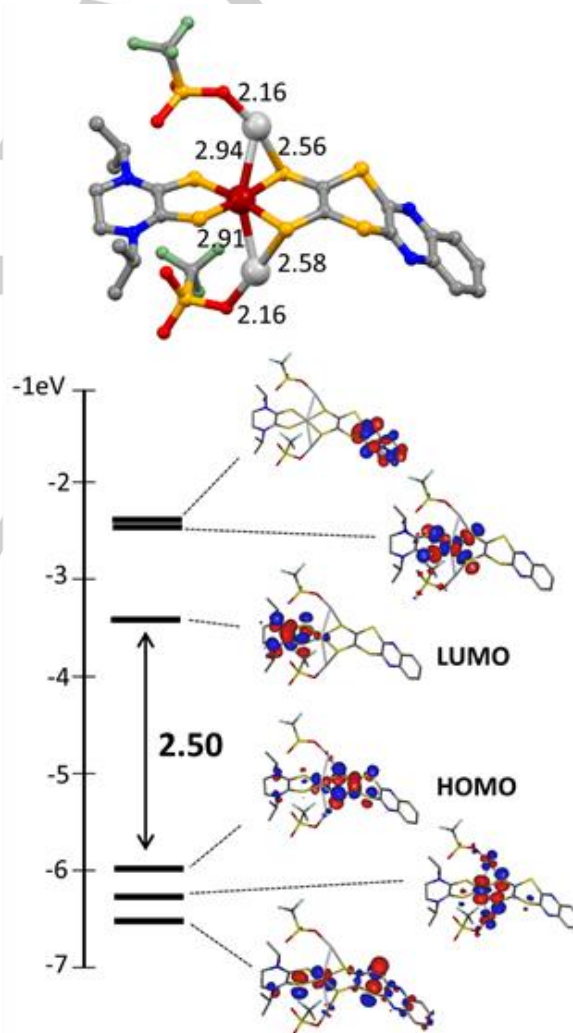


Figure 9: Above, optimized molecular structure of the adduct **3a-2(AgCF₃SO₃)** in the gas phase (B3LYP/6-31+G(d)-SDD). Selected bond distances are reported in Å. Below, selected frontier molecular orbitals.

FULL PAPER

materials with tunable emission and NLO properties. In this report, we have detailed the synthesis and physical characterization of the [Pt(i-Pr₂pipdt)(Quinoxdt)] complex (**3a**) and of the corresponding Ni and Pd derivatives inside the triad. These complexes, characterized by the presence of an acceptor and a donor ligands at the opposite side of the M(II) center, show negative solvatochromic absorption and high second-order polarizability relatable to CT donor-acceptor transition. **3a** shows uncommon room temperature emission. In fact, after the excitation at 440 nm, the observed emission is found at 570 nm, which is significantly higher in energy than the low-energy absorption (836 nm). This process is in line with a potential anti-Kasha behaviour of the complexes. Addition of silver triflate produces the formation of a **3a**:Ag(I) 1:2 adduct, with significant change of the optical properties, that is hypsochromic shift of the lowest absorption band, and the emission is quenched. Upon addition of silver triflate, the luminescence is restored. Similar behaviour is observed for the corresponding Ni(II) derivative while the Pd(II) one is non-emissive. Computational studies have provided a crucial contribution to support the interpretation of the observed properties. The Fukui functions indicated the preferential sites of interaction with incoming electrophile or nucleophile, and in particular with a soft metal ion such as Ag(I). According to these computations, the thiolic sulfur atoms and to a minor extent the Pt center are the preferential sites of interaction with the silver ions. In addition, the comparison of the properties of **3a** with those of [Pt(i-Pr₂pipdt)(dmit)], and of [Pt(MBA)(Quinoxdt)]⁺Cl⁻ shows that all the complexes exhibit high second order NLO activity, but only those which bear the Quinoxdt ligand emit with a high quantum yield. The DFT calculations of the d-orbitals sequence in non-emitting complexes (including silver adduct of **3a**) shows that the metal-centered d_{xy}* orbital is lowered in energy with respect to the d* ligand orbital, likely providing an efficient non-radiative d-d decay channel.^[16]

Collective observations supported by computational studies enabled us to shed light on the steric-electronic influence of substituted dithiolene ligands (R, R = Quinoxdt) on the relevant optical properties, such as the unique emission behaviour of this class of complexes.

Experimental Section

Synthesis. Reagents and solvents were purchased from Aldrich and used without further purification. Complex **4** was prepared following ref. 3b and ligand **5** was prepared according to ref. 24.

[Pt(iPr₂pipdt)(Quinoxdt)] (3a): A solution of sodium (7.9 mg, 3.46 mmol) in 10mL of methanol was added to a suspension of **5** (48.5 mg, 1.57 mmol) in 50% MeOH/CHCl₃ mixture and stirred at room temperature for 30 minutes. The brown solution of dithiolate formed was added drop-wise to a reddish solution of **4** (78 mg, 1.57 mmol) in 200mL of 15% MeOH/CHCl₃. The reaction mixture was then refluxed overnight to obtain green microcrystalline [Pt(i-Pr₂Pipdt)(Quinoxdt)] (**3a**) (96mg, 86%) which was collected by centrifugation followed by washing with diethyl ether. Well-formed crystals suitable for single crystal XRD studies were obtained through re-crystallization by diffusion from DMF/diethyl ether. UV-vis (DMF solution): λ_{max} (nm) ε (mol cm⁻¹ dm⁻³): 369 (1.73×10⁴); 465sh

(3.8×10³); 836 (1.05×10⁴). FT. IR: ν_{max} cm⁻¹: 3106 (vw); 3062 (vw); 2930 (w); 2858 (w); 1664, 1609 (s-ms), bCO DMF; 1503 (s), bCN i-Prpipdt; 1357 (ms), bCC quinoxdt; 1264 (ms); 1177 (s); 1111 (vs); 1050 (ms); 959 (m); 854 (ms); 762 (s); 658 (m); 597 (s). ¹H NMR [(CD₃)₂SO] X: 7.96 (CH, 1H, s DMF); 7.90 (CH, 2H m) 7.75 (CH 2H m); 5.15 (CH 1H m), 4.92 (CH 1H m); 3.75 (CH₂ 2H s); 2.89-2.73 (CH₃ 3H s - CH₃ 3Hs DMF); 1.48 (CH₃) 6H d 1.35 (CH₃) 6H d (the other signal of the CH₂ protons of the pip ring is likely covered by the peak at 3.25-3.35 ppm arising from water). Peaks at 1.1 (CH₃), 1 H t, and 3.4 CH₂, 0.8 H q, shows the presence of adsorbed Et₂O). XRD patterns of **3a** powders are consistent with single crystal data of **3a** as shown in Figure S11.

Measurements

IR spectra (4000–400 cm⁻¹) were recorded with a Bruker Tensor 27 Platinum ATR. ¹H-NMR spectra were performed on Bruker 500 MHz at room temperature. Electronic absorption spectra were recorded with an Agilent Cary 5000 spectrophotometer. X-ray Powder Diffraction measurements were performed on a Panalytical Empyrean diffractometer equipped with a graphite monochromator on the diffracted beam and an X'Celerator³ detector. The scan rate was 0.5°/min. The data were collected within the range of 4°–80° (2θ) using CuKα radiation.

Experimental single crystal X-ray

A summary of data collection and structure refinement for [Pt(i-Pr₂pipdt)(quinoxdt)]·DMF is reported in Table 1. Single crystal data were collected with a Bruker Smart APEXII at 240 K (Mo Kα, λ = 0.71073 Å). The intensity data were integrated from several series of exposures frames (0.3° width) covering the sphere of reciprocal space.^[25] Absorption correction were applied using the program SADABS.^[26] The structures were solved by the dual space algorithm implemented in the SHELXT code.^[27] Fourier analysis and refinement were performed by the full-matrix least-squares methods based on F₂ implemented in SHELXL-2014.^[28] Graphical material was prepared with the Mercury 3.9 program.^[29] CCDC 1833235 contains the supplementary crystallographic data for this paper.

Computational studies

The electronic properties of [Pt(i-Pr₂pipdt)(quinoxdt)] were investigated by means of DFT methods.^[30] The molecular structure of the complex was optimized starting from the experimental geometry derived by the X-ray structural characterization using no symmetry constraints. The Becke three-parameter exchange functional with Lee-Yang-Parr correlation functional (B3LYP)^[31, 32] was employed together with the 6-31+G(d) basis set for the C, H, N, and S atoms.^[33, 34] The Pt atom was treated and SDD valence basis set^[35, 36, 37] and with the MWB60 effective core potentials in order to take into account relativistic effects. To address acetonitrile solvation effects, the polarisable continuum model (PCM) was applied during the single point calculations using gas-phase optimized geometries.^[38] The first twenty singlet-singlet vertical excitation energies of [Pt(i-Pr₂pipdt)(quinoxdt)] were determined using time-dependent density functional theory (TD-DFT).^[39, 40] Also for these calculations, the contribution of the solvent was taken into account by the PCM method. The dipole moment difference between the excited and ground states (Δa_{ge} = |6.9 Debye) was calculated by using the finite field approach (external field strength of 0.001 atomic units). Fukui functions^[9, 19, 41] were computed by taking the difference of the electron density of the N+1 and N system, f₊ = ρ(N+1) - ρ(N), and the difference between the electron density of the N and N-1 system, f₋ = ρ(N) - ρ(N-1) (N = number of electrons) using the optimized geometry of the neutral species (N). All the calculations were performed with the Gaussian 03 program suite.^[42]

FULL PAPER

Molecular orbital diagrams and isodensity surfaces were generated with the Gabedit program.^[43] AOMix was used to analyze the electronic transitions obtained from TD-DFT calculations.^[44]

Photoluminescence studies.

Emission spectra were collected with a Horiba-Jobin Yvon Fluoromax-4 Spectrofluorimeter using a 400W Xenon lamp. All spectra were corrected for detector response. Appropriate optical filters were used. Band pass was set as 10 nm slit width for each measurement. Solvent contribution was subtracted for all absorbance/emission spectra. Emission quantum yield was evaluated using the relative method through the following equation:

$$\Phi = \Phi_R \times (a_R/a) \times (I/I_R) \times (n/n_R)^2$$

where the R index refers to the photoluminescence standard. Φ_R = reference quantum yield; $a_R=10^4 A$, absorption factor of the reference at excitation wavelength; $a=10^4 A$, absorption factor of the sample at excitation wavelength; A_R =absorbance of the reference at excitation wavelength; A =absorbance of the sample at excitation wavelength; I =sample integrated emission; I_R =reference integrated emission; n =refractive index of the medium. $[Ru(bpy)_3]^{2+}$ was used as suitable reference standard.

Second-order Nonlinear Optical Properties

The second order NLO responses of the molecular chromophore was measured by the EFISH (Electric Field Induced Second Harmonic generation) technique, which provides the χ_{EFISH} value, from which EFISH quadratic hyperpolarizability can be obtained through eq. 1

$$\chi_{EFISH} = (\mu\beta / 5KT) + \frac{1}{2} \frac{A^2}{L^2} \frac{1}{\omega} \frac{1}{\omega} \frac{1}{\omega} \dots (1)$$

where μ is the ground state dipole moment, $\beta / 5KT$ the dipolar orientational contribution, A is the fundamental wavelength of the incident photons in the EFISH experiment, L is the length of the incident photons, ω is the frequency of the incident photons, corresponding to the cubic contribution to χ_{EFISH} , usually negligible for dipolar chromophores such as this studied in this work. Finally, χ_{EFISH} is the projection along the dipole moment axis of the vectorial component χ_{vec} of the tensorial quadratic hyperpolarizability. In the following χ_{EFISH} is reported as χ_{1907} since the EFISH experiments were carried out working with a 1907 nm non resonant incident wavelength. All the EFISH measurements were carried out in DMF solutions at 10^{-3} M concentration and the experimental χ_{1907} values obtained are the averages of 16 measurements. All experimental EFISH χ_{1907} values are $\chi_{1907} = \chi_{vec} \cdot \cos^2 \theta$ where θ is the angle between the incident laser beam and the dipole moment axis.^[45]

Acknowledgements

Università degli Studi di Cagliari and Regione Autonoma della Sardegna are acknowledged for supporting this research through Premialità PRIN 2016. The authors are grateful to Dr Flaminia Cesare Marincola for NMR spectra. F.A. gratefully acknowledges the Research Foundation Flanders (FWO) and the Curie research and innovation programme (ANR-17-CE30-0010-01) and the Curie grant, agreement No 665501.

Keywords: Dithiolenes • Optical Properties • Crystal Structure • DFT calculations • Platinum

- [1] a) A. Das, Z. Han, W. W. Brennessel, P. L. Holland, R. Eisenberg, *ACS Catalysis* **2015**, *5*, 1397-1406; b) R. Kato, *Chem. Rev.* **2004**, *104*, 5319-5346; c) G. C. Anyfantis, G. C. Papavassiliou, N. Assimomytis, A. Terzis, V. Psycharis, C. P. Raptopoulou, P. Kyritsis, V. Thoma, I. B. Koutselas, *Solid State Sciences* **2008**, *10*, 1729-1733.
- [2] P. Deplano, D. Espa, M. L. Mercuri, L. Pilia, A. Serpe, *Coord. Chem. Rev.* **2010**, *254*, 1434-1447.
- [3] a) D. Espa, L. Pilia, C. Makedonas, L. Marchioli, M. L. Mercuri, A. Serpe, A. Barsella, A. Fort, C. A. Mitsopoulou, P. Deplano, *Inorg. Chem.* **2014**, *53*, 1140-1147; b) D. Espa, L. Pilia, A. Barsella, A. Fort, S. J. Dalgleish, N. Robertson, P. Deplano, *Inorg. Chem.* **2011**, *50*, 2058-2060.
- [4] a) A. Iuris, P. Deplano et al. unpublished results; b) F. Frei, A. Rondi, D. Espa, M. L. Mercuri, L. Pilia, A. Serpe, A. Odeh, F. Van Mourik, M. Chergui, *Dalton Trans.* **2014**, *43*, 17666-17676.
- [5] M. Hissler, J. E. McGarrah, W. B. Connick, D. K. Geiger, S. D. Cummings, R. Eisenberg, *Coord. Chem. Rev.* **2000**, *208*, 115.
- [6] M. Kasha, *Discuss. Faraday Soc.* **1950**, 91-101.
- [7] S. Attar, D. Espa, F. Artizzu, M. L. Mercuri, A. Serpe, E. Sessini, G. Concas, F. Congiu, L. Marchioli, P. Deplano, *Inorg. Chem.* **2016**, *55*, 5118-26.
- [8] S. Attar, D. Espa, F. Artizzu, L. Pilia, A. Serpe, M. Pizzotti, G. Di Carlo, L. Marchioli, P. Deplano, *Inorg. Chem.* **2017**, *56*, 1111-1118.
- [9] R. G. Parr, W. Yang, *J. Am. Chem. Soc.* **1984**, *106*, 4049-4050.
- [10] a) D. Espa, L. Pilia, L. Marchioli, F. Artizzu, A. Serpe, M. L. Mercuri, D. Simão, M. Almeida, M. Pizzotti, F. Tessore, P. Deplano, *Dalton Trans.*, **2012**, *41*, 3485-3493; b) L. Pilia, D. Espa, A. Barsella, A. Fort, C. Makedonas, L. Marchioli, M. L. Mercuri, A. Serpe, C. A. Mitsopoulou, P. Deplano, *Inorg. Chem.* **2011**, *50*, 10015-10027; c) D. Espa, L. Pilia, L. Marchioli, S. S. Attar, A. Barsella, A. Fort, M. L. Mercuri, A. Serpe, P. Deplano, *CrystEngComm* **2015**, *17*, 4161-4171.
- [11] a) S. D. Cummings, R. Eisenberg, *J. Am. Chem. Soc.* **1996**, *118*, 1949-1960; b) S. D. Cummings, L.-T. Cheng, R. Eisenberg, *Chem. Mater.* **1997**, *9*, 440-450.
- [12] a) C. Mitsopoulou, *Coord. Chem. Rev.* **2010**, *254*, 1448-1456; b) E. A. M. Geary, L. J. Yellowlees, L. A. Jack, I. D. H. Oswald, S. Parsons, N. Hirata, J. R. Durrant, N. Robertson, *Inorg. Chem.* **2005**, *44*, 242-250.
- [13] Although spectral range instrumental limits may hamper the direct observation of emission in the near-infrared region (>850 nm) in this case, we can compare the spectral properties with those the analogous compound **2**. In the latter, the lowest-lying absorption band falls below 600 nm and allows photoluminescence investigation up to the near-infrared (~900 nm) without the interference of inner filter effects (mainly due to re-absorption). The absence of any detectable emission in the near-infrared following excitation in the lowest HOMO-LUMO band in **2**, provides, by analogy, further support to the apparent anti-Kasha behaviour of **3a**.
- [14] T. R. Miller, G. Dance, *J. Am. Chem. Soc.* **1973**, *95*, 6970.
- [15] M. A. Mansour, R. J. Lachicotte, H. J. Gysling, R. Eisenberg, *Inorg. Chem.* **1998**, *37*, 4625.
- [16] S. D. Cummings, R. Eisenberg in *Dithiolenes Chemistry: synthesis, Properties and Applications, Progress in Inorganic Chemistry*, Vol. 52 (Eds.: E. I. Stiefel, John Wiley & Sons, Inc), **2004**, pp. 316-367.
- [17] F. Julii, P. Jones, P. Gonzi lez-Herrero, *Inorg. Chem.* **2012**, *51*, 5037.
- [18] J. Moussa, L.M. Chamoreau M.P. Gullo, A. Degli Esposti; A. Barbieri, H. Amouri, *Dalton Trans.* **2016**, *45*, 2906.
- [19] *Chemical Reactivity Theory: A Density Functional View*, CRC press, 2009, Ed. P. K. Chattaraj
- [20] S. S. Batsanov, *Inorganic Materials*, **2001**, *37*, 871-885.
- [21] R. S. Pilato, K. A. Van Houten in *Dithiolenes Chemistry: synthesis, Properties and Applications, Progress in Inorganic Chemistry*, Vol. 52, (Eds.: E. I. Stiefel, John Wiley & Sons, Inc) **2004**, pp. 369-397.

FULL PAPER

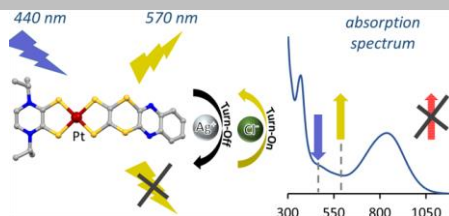
- [22] J. L. Oudar, D. S. Chemla, *J. Chem. Phys.* **1997**, *66*, 2664.
- [23] S. Bruni, E. Cariati, F. Cariati, F. A. Porta, S. Quici, D. Roberto, *Spectrochim. Acta, Part A*, **2011**, *57*, 1417-1426.
- [24] L. Hu, J. Qin, N. Zhou, Y.-F. Meng, Y. Xu, J.-L. Zuo, X.-Z. You, *Dyes Pigm.* **2012**, *92*, 1223.
- [25] (SMART (control) and SAINT (integration) software for CCD systems; Bruker AXS: Madison, WI, 1994)
- [26] (Area-Detector Absorption Correction; Siemens Industrial Automation, Inc.: Madison, WI, 1996)
- [27] G. M. Sheldrick, *Acta Crystallographica Section A*, **2005**, *71*, 3-8
- [28] G. M. Sheldrick, *Acta Crystallographica Section C*, **2005**, *71*, 3-8.
- [29] C. F. Macrae, P. R. Edgington, P. McCabe, E. Pidcock, G. P. Shields, R. Taylor, M. Towler, J. J. van de Streek, *Appl. Crystallogr.* **2006**, *39*, 453-457.
- [30] R. G. Parr, W. Yang in *Density-Functional Theory of Atoms and Molecules*, (Ed. Oxford University Press), New York, **1989**.
- [31] A. D. Becke, *Physical Review A: Atomic, Molecular, and Optical Physics*, **1988**, *38*, 3098-3100.
- [32] A. D. Becke, *Journal of Chemical Physics* **1993**, *98*, 5648-5652.
- [33] R. Ditchfield, W. J. Hehre, J. A. Pople, *J. Chem. Phys.* **1971**, *54*, 724.
- [34] V. A. Rassolov, M. A. Ratner, J. A. Pople, P. C. Redfern, L. A. Curtiss, *J. Comp. Chem.* **2001**, *22*, 976.
- [35] P. Fuentealba, H. Preuss, H. Stoll, L. v. Szentpaly, *Chem. Phys. Lett.* **1989**, *89*, 418.
- [36] X. Y. Cao, M. Dolg, *J. Mol. Struct. (Theochem)* **2002**, *581*, 139.
- [37] P. Schwerdtfeger, M. Dolg, W. H. E. Schwarz, G. A. Bowmaker, P. D. W. Boyd, *J. Chem. Phys.* **1989**, *91*, 1762.
- [38] B. Mennucci, J. Tomasi, *J. Chem. Phys.* **1997**, *106*, 5151.
- [39] M. E. Casida, C. Jamorski, K. C. Casida, D. R. Salahub, *Journal of Chemical Physics* **1998**, *108*, 4439-4449.
- [40] R. E. Stratmann, G. E. Scuseria, M. J. Frisch, *Journal of Chemical Physics* **1998**, *109*, 8218-8224.
- [41] K. Fukui, *Science* **1982**, *218*, 747-784.
- [42] Gaussian 03, Revision C.02, M. J. Frisch, G. W. Trucks, H. B. Schlegel, G. E. Scuseria, M. A. Robb, J. R. Cheeseman, Jr., J. A. Montgomery, T. Vreven, K. N. Kudin, J. C. Burant, J. M. Millam, S. S. Iyengar, J. Tomasi, V. Barone, B. Mennucci, M. Cossi, G. Scalmani, N. Rega, G. A. Petersson, H. Nakatsuji, M. Hada, M. Ehara, K. Toyota, R. Fukuda, J. Hasegawa, M. Ishida, T. Nakajima, Y. Honda, O. Kitao, H. Nakai, M. Klene, X. Li, J. E. Knox, H. P. Hratchian, J. B. Cross, V. Bakken, C. Adamo, J. Jaramillo, R. Gomperts, R. E. Stratmann, O. Yazyev, A. J. Austin, R. Cammi, C. Pomelli, J. W. Ochterski, P. Y. Ayala, K. Morokuma, G. A. Voth, P. Salvador, J. J. Dannenberg, V. G. Zakrzewski, S. Dapprich, A. D. Daniels, M. C. Strain, O. Farkas, D. K. Malick, A. D. Rabuck, K. Raghavachari, J. B. Foresman, J. V. Ortiz, Q. Cui, A. G. Baboul, S. Clifford, J. Cioslowski, B. B. Stefanov, G. Liu, A. Liashenko, P. Piskorz, I. Komaromi, R. L. Martin, D. J. Fox, T. Keith, M. A. Al-Laham, C. Y. Peng, A. Nanayakkara, M. Challacombe, P. M. W. Gill, B. Johnson, W. Chen, M. W. Wong, C. Gonzalez, J. A. Pople, Gaussian, Inc., Wallingford CT, **2004**
- [43] A. R. Allouche, *Journal of Computational Chemistry* **2011**, *32*, 174-182.
- [44] S. I. Gorelsky, AOMix: Program for Molecular Orbital Analysis, <http://www.sg-chem.net/>, version 6.52, **2011**.
- [45] A. Willetts, J. E. Rice, D. M. Burland, D. P. Shelton, *J.Chem.Phys.* **1992**, *97*, 7590-7599.

FULL PAPER

Entry for the Table of Contents

FULL PAPER

The uncommon optical properties of the depicted compound: apparent anti-Kasha emission, switchable for silver addition/removal, and 2nd NLO activity, are elucidated here by combined experimental and theoretical studies.



Salahuddin S. Attar, Flavia Artizzu, Luciano Marchiò, * Davide Espa, Luca Pilia, Maria F. Casula, Angela Serpe, Maddalena Pizzotti, Alessio Orbelli Biroli and Paola Deplano*

Page No. – Page No.

Uncommon Optical Properties and Silver-responsive Turn-off/on Luminescence in a Pt(II) heteroleptic dithiolene complex.